A NEW INSIGHT INTO THE POSITION OPTIMIZATION OF WAVE ENERGY CONVERTERS BY A HYBRID LOCAL SEARCH

A PREPRINT

Mehdi Neshat
Optimization and Logistics Group
School of Computer Science
The University of Adelaide
Australia
mehdi.neshat@adelaide.edu.au

Bradley Alexander
Optimization and Logistics Group
School of Computer Science
The University of Adelaide
Australia
bradley.alexander@adelaide.edu.au

Nataliia Y. Sergiienko
School of Mechanical Engineering
The University of Adelaide
Australia
nataliia.sergiienko@adelaide.edu.au

Markus Wagner
Optimization and Logistics Group
School of Computer Science
The University of Adelaide
Australia
markus.wagner@adelaide.edu.au

April 23, 2019

ABSTRACT

Renewable energy, such as ocean wave energy, plays a pivotal role in addressing the tremendous growth of global energy demand. It is expected that wave energy will be one of the fastest-growing energy resources in the next decade, offering an enormous potential source of sustainable energy. This research investigates the placement optimization of oscillating buoy-type wave energy converters (WEC). The design of a wave farm consisting of an array of fully submerged three-tether buoys is evaluated. In a wave farm, buoy positions have a notable impact on the farm's output. Optimizing the buoy positions is a challenging research problem because of very complex interactions (constructive and destructive) between buoys. The main purpose of this research is maximizing the power output of the farm through the placement of buoys in a size-constrained environment. This paper proposes a new hybrid approach of the heuristic local search combined with a numerical optimization method that utilizes a knowledge-based surrogate power model. We compare the proposed hybrid method with other state-of-the-art search methods in five different wave scenarios – one simplified irregular wave model and four real wave climates. Our method considerably outperforms all previous heuristic methods in terms of both quality of achieved solutions and the convergence-rate of search in all tested wave regimes.

Keywords Renewable energy · Evolutionary Algorithms · Position Optimisation · Hybrid Local Search · knowledge-based surrogate model · Wave Energy Converters

1 Introduction

Wave energy converters (WECs) have attracted research and industry interest because of their high capacity factors and energy densities relative to other renewable energy sources [1]. There are a number of alternative designs for WECs, but one of the current-best designs is a large floating buoy tethered to the sea floor with energy produced by the motion of the buoy exerting force on the tether. Wave-energy farms, consisting of multiple buoys, are able to extract power from the waves more than 90% of the time; this is in contrast to solar and wind power, which have much higher levels of intermittency [1].

In addition, WECs are able to take advantage of the high energy-density of marine environments – up to 60 kW per square meter with a very low impact on aquatic life [2].

The amount of power produced by a farm or an array of WECs depends on their arrangement with respect to each other and the prevailing wave conditions at the test site. Thus, generating the appropriate arrangement of WECs in an array is an important factor in maximizing power absorption. Previous work [3] has identified four factors that link array layout in a farm to energy production: (1) number of converters, (2) the distance between the converters, (3) the array layout, and (4) the wave directions.

Current designs for WECs produce up to 1 MW per buoy [4]. Thus, to be of commercial scale, it is necessary for farms to consist of multiple buoys. However, as the number of converters is increased, the optimization of buoy placement becomes more challenging because of complex hydrodynamic interactions among converters. These interactions can be constructive or destructive, and the geometry of these interactions depends strongly on the prevailing wave regime in the environment. In evaluating potential layouts, it is important to use an energy-model that has both high-fidelity and simulates the best available WEC designs. The model used here [5] uses a detailed model for the wave regime at a given location, including information on wave height, frequency, and direction. The model simulates a fully-submerged three-tether WEC which extracts more energy than the previous single-tether design.

The search space for optimizing array layouts for these WECs is non-convex and multi-modal. Evaluation of each layout is expensive, sometimes taking several minutes, because of complex and extensive hydrodynamic interactions between buoys, which are dependent on the local conditions.

The nature of this search space requires the application of search meta-heuristics that reliably explore these multi-modal search landscapes, that can also operate effectively with a constrained number of layout evaluations. To date, works on WEC array layouts have primarily employed evolutionary algorithms (EAs), which combine stochastic search with selection to progressively improve a population of candidate layouts. In early work [6], Child and Venugopal applied both a simple (and deterministic) Parabolic Intersection (PI) heuristic and a more computationally intensive Genetic Algorithm (GA) to create small (five-buoy) WEC layouts.

Later work by Sharp and DuPont [7] used a GA, coupled with heuristics to ensure minimum separation between buoys, to place a small number of WECs (5 converters, 37000 evaluations) in a discretized space. The same authors later explored a similar problem with an improved GA with a cost model [8]. In both studies, the wave-model used assumed a single wave direction, which can limit its applicability. The studies also required a relatively large number of layout evaluations, which would be costly in a setting that uses more detailed models.

An alternative approach is proposed by Ruiz et al. [9], who compare the convergence rate and efficiency of three EAs in a discrete search space with a simple wave energy model. The EAs included: CMA-ES [10], a custom GA, and glow-worm swarm optimization (GSO) [11]. Their work found that search using CMA-ES converged faster than other methods but was out-performed, in terms of energy production by both the GA and GSO.

In other studies, Wu et al. [12] investigated two popular EAs: the 1+1EA and CMA-ES for optimizing the locations of fully submerged three-tether buoys. The results show the performance of 1+1EA with a simple mutation operator is better than CMA-ES when constrained to a very limited number of layout evaluations. The same wave model was used by Arbones et al. [13, 14] in a multi-objective optimization problem. In that study, two multi-objective optimization methods (MO-CMA-ES and SMS-EMOA) are applied to acquire the best trade-offs of the converter positions, the farm area and the cable length needed. However, again, a very simple wave model with just one wave frequency and direction are simulated, so the results can diverge from a more realistic wave climate.

A much more detailed wave scenario was applied in Neshat et al. [15]. They used an irregular wave model with seven wave directions and fifty sampled wave frequencies, to evaluate a wide variety of EAs and hybrid methods. This work found that a combination of a stochastic local search combined with the Nelder-Mead simplex method can obtain better 4 and 16-buoy configurations in terms of the total absorbed power. However, the optimization process was still computationally intensive taking 72 hours on 12 CPU cores, and the model used was still for a synthetic location. Furthermore, A multi-objective differential evolutionary (DE) was proposed for optimizing the geometric parameters of WECs like PTO, location, control strategy type of a doubled-buoy WEC [16].

This paper improves on prior work in the following ways: augmenting the findings of [15] to include another six new heuristic search methods, including a novel surrogate-based model, all applied to the original irregular wave model; extending the wave models to include four new real wave regimes from the southern coast of Australia (Adelaide, Perth, Tasmania and Sydney) using a higher granularity of wave-directions; finally, the best of the new search methods are applied to the four real wave models.

In comparing the performance of the new search heuristics, we consider two aspects: the computational budgets and the quality of achieved layouts. Through this comparison, we show that a hybrid framework consisting of a learned

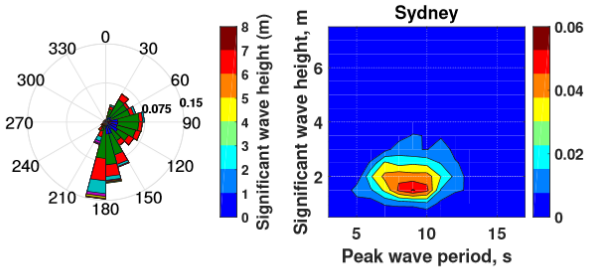

(a)

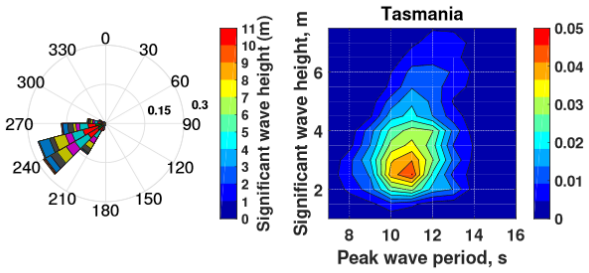

(b)

Figure 1: Wave data for two test sites in Australia: (a) Sydney and (b) Perth. These are: the directional wave rose (left) and wave scatter diagram (right).

model-based local search alternated with numerical optimization outperforms previous heuristic methods in terms of convergence rate (20-fold faster than the previous best method in [15]) and higher total power output for 16-buoy and 4-buoy layouts.

The paper structure is as follows. In the next section, the buoy model is described. The optimization problem is defined in the second section and the search methods to be compared are briefly described in the third section. In the fourth section, experimental results are evaluated, and the final section discusses these results and canvases future work.

2 The Numerical Model

2.1 Wave Resource

Four potential sites on the southern coast of Australia are considered in this study: Adelaide, Perth, Tasmania (southwest coast) and Sydney. The wave regimes for the Sydney and Tasmania sea sites are shown in Figure 1 demonstrating the directional wave rose and wave scatter diagram. These wave data are obtained from the Australian Wave Energy Atlas [17]. It can be observed that these wave regimes vary in terms of total energy, and directional distributions of the waves. For the wave farm optimization purposes, ocean waves are modeled as directional irregular waves assuming Bretschneider spectrum.

2.2 Wave Energy Converter Description

A wave energy converter considered in this study is shown in Fig. 2. This converter consists of a fully submerged spherical buoy connected to three independent power take-off units through inclined taught tethers. This design represents a simplified prototype of the CETO system under development by Carnegie Clean Energy [4][18]. The parameters of the WEC are specified in Table 1.

It is assumed that the motion of each WEC is constrained to three degrees of freedom (surge, sway and heave). Assuming linear wave theory, the equation of motion of all wave energy converters in the farm can be written in frequency domain as:

$$\left(-(\mathbf{M}+\mathbf{A})\omega^2+(\mathbf{B}+\mathbf{B}_{pto})j\omega+\mathbf{K}_{pto}\right)\mathbf{x}=\mathbf{F}_{exc}, \tag{1}$$

where $\mathbf{M}=m\mathbf{I}_{3N}$ is a mass matrix ($\mathbf{I}_{3N}$ is the identity matrix of size $3N$), $\mathbf{A}$ and $\mathbf{B}$ are the matrices of hydrodynamic added-mass and radiation damping coefficients respectively, $\mathbf{K}_{pto}=K_{pto}\mathbf{I}_{3N}$ and $\mathbf{B}_{pto}=B_{pto}\mathbf{I}_{3N}$ are the PTO stiffness and damping matrices respectively, and $\mathbf{F}_{exc}$ is the frequency dependent vector of excitation forces. All the

Table 1: Key parameters for WECs simulated in this research

Parameter	Value
Buoy number	4, 16
Buoy radius	5 m
Submergence depth (top of WEC)	3 m
Water depth	50 m
Buoy mass, m	376 tonnes
Buoy volume	523.60 m^3
Tether angle	55°
PTO stiffness, K_{pto}	2.7×10^5 N/m
PTO damping, B_{pto}	1.3×10^5 Ns/m

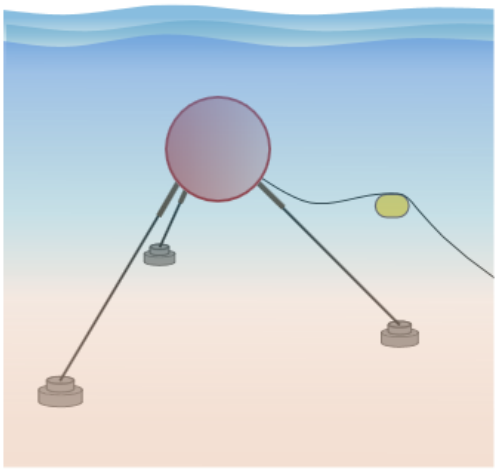

Figure 2: The applied WECs model

matrices have dimensions $(3N \times 3N)$, where 3 represents the number of degrees of freedom of each WEC and N is a number of WECs in the farm. The hydrodynamic interaction between submerged spheres, in particular matrices $\mathbf{A}, \mathbf{B}$ and vector $\mathbf{F}_{exc}$, are modeled using a semi-analytical solution presented in [19].

The average power absorbed by all WECs in the farm in a regular wave of unit amplitude, wave frequency ω and wave angle β can be calculated as:

$$P(\beta,\omega) = \frac{\omega^2}{2}\mathbf{x}^T(\beta,\omega)\mathbf{B}_{pto}\mathbf{x}(\beta,\omega), \tag{2}$$

where $\mathbf{x}(\beta,\omega)$ is obtained solving Eq. (1).

2.3 Wave Farm Performance Evaluation

The total average annual power (P_Σ) produced by the wave farm at a particular test site is calculated by summing up the contribution of energy absorption from each of the sea states representing a wave climate:

$$P_\Sigma = \sum_{n=1}^{N_s} O_n(H_s,T_p)P_n(H_s,T_p), \tag{3}$$

where N_s is a number of sea states considered, H_s is the significant wave height, T_p is the peak wave period of the sea state, $O_n(H_s,T_p)$ is the probability of occurrence of the sea state (which can be derived from the wave scatter diagram), and $P_n(H_s,T_p)$ is a power generated by the wave farm in the n-th sea state. A sea state refers to the condition of the sea/ocean surface that can be characterized by statistics (significant wave height and peak wave period).

For irregular waves, $P_n(H_s,T_p)$ is the sum of power contribution from each frequency in the spectrum and each wave direction [20]:

$$P_n(H_s,T_p) = \int_0^{2\pi}\int_0^{\infty} 2S_n(\omega)D(\beta)p(\beta,\omega)\mathrm{d}\omega\mathrm{d}\beta, \tag{4}$$

where $p(\beta,\omega)$ is the average power absorbed by the wave farm in a regular wave of unit amplitude, wave frequency ω and wave angle β (calculated according to [21]), $S_n(\omega)$ is the irregular wave spectrum (Bretschneider spectrum

considered in this study) and $D(\beta)$ is the directional spreading spectrum specific for the site (obtained from the directional wave rose).

The hydrodynamic interaction among converters in the wave array affects its power production and is usually quantified using the q-factor, defined as:

$$q = \frac{P_\Sigma}{NP_{isolated}}, \tag{5}$$

where N is a number of WECs forming the array, $P_{isolated}$ is the power generated by an isolated WEC. If the wave interaction has on average a constructive effect on the power production of the array, then $q > 1$, and if the effect is destructive then, $q < 1$.

Initially, all optimization algorithms are evaluated using a simplified synthetic wave model that corresponds to the most frequently occurring sea state at the Sydney site ($H_s = 2$ m, $T_p = 9$ sec) using Equation (4). Then, the proposed ideas are tested for four real wave scenarios using Equation (3).

3 Optimization Setup

Using the above model, the optimization problem can be stated in terms of positioning N WECs over a bounded area of a wave farm Ω in order to maximize the total power production P_Σ.

$$\begin{aligned} & P^*_\Sigma = \mathit{argmax}_{\mathbf{x},\mathbf{y}} P_\Sigma(\mathbf{x_i}, \mathbf{y_i}) \\ & \text{Subject to} \\ & \quad [x_i, y_i] \in \Omega, \quad i = 1, ..., N \\ & \quad \mathit{dist}((x_i, y_i), (x_j, y_j)) \geq R' \quad i \neq j = 1, ..., N \end{aligned} \tag{6}$$

Where $P_\Sigma(\mathbf{x}, \mathbf{y})$ is the sum of mean power output by buoys positioned in an area at x-positions $\mathbf{x} = [x_1, \ldots, x_N]$ and corresponding y positions $\mathbf{y} = [y_1, \ldots, y_N]$. In this study, the maximum number of buoys is predefined to be $N = 4$ and $N = 16$. For each buoy the coordinate: $[x_i, y_i]$ is the position of the i^{th} buoy. This position is constrained to be within the area Ω. Where $\Omega = l \times w$ and $l = w = \sqrt{N * 20000}\, m$. This constraint is given to model the scenario where there are strict limits on the area allotted to a wave farm lease. A second constraint is a minimum separation between buoys ($R' = 50m$), representing a gap required for maintenance vessels to safely pass. For each array, $\mathbf{x}, \mathbf{y}$ the sum-total of the safety distance violations are:

$$\begin{aligned} \mathit{Sum}_{\mathit{dist}} = \textstyle\sum_{i=1}^{N-1} \sum_{j=i+1}^{N} (\mathit{dist}((x_i, y_i), (x_j, y_j)) - R', \\ \text{if } \mathit{dist}((x_i, y_i), (x_j, y_j)) < R' \text{ else } 0 \end{aligned}$$

Where $\mathit{dist}((x_i, y_i), (x_j, y_j))$ is the Euclidean distance between buoys i and j. To provide a smooth response to such violations, a steep penalty function $(\mathit{Sum}_{\mathit{dist}} + 1)^{20}$ is applied to the total power output (in Watts).

3.1 Computational Resources

A common practice in comparing heuristic search methods is to run competing methods for the same number of function evaluations. However, such a comparison is not applicable in this paper, because the computational cost of each function evaluation (layout assessment) depends strongly on the number of buoy interactions and wave frequencies models – both of which vary with the search methods examined here. Instead, in this work, to compare methods fairly we allocate a uniform time budget for each optimization run of three days on the dedicated platform with a 2.4GHz Intel 6148 processor running 12 processes in parallel with 128GB of RAM. The software environment running the function evaluations and the search algorithm is MATLAB R2016.

Where practical, the search methods are each configured to make maximum use of this time budget where the algorithm design allows this. This means that for some search methods the parallelism is expressed in terms of parallel evaluations of members of a population of individual layouts. In non-population based (single-solution) methods, the parallelism is expressed through parallel evaluation of the energy extracted from wave-frequencies. In this way, each method is allowed to achieve an approximately 10-fold speedup, compared to the corresponding sequential algorithms, on the parallel processor.

There are two exceptions to this principle of maximally using the time budget. These are the (best performing) Smart Local Search (SLS) and the Improved Smart Local Search (ISLS) methods. The local optimization steps for both these

methods converge quickly and their results are not substantially improved by allocating more search time. To allow for a valid statistical comparison all search methods are run 10 times.

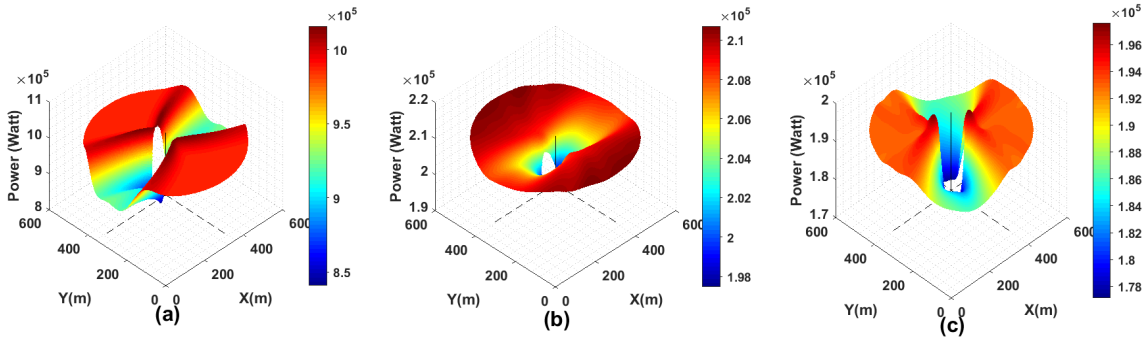

Figure 3: The 3D power landscape of two-buoy array based on the simplified irregular (a), Sydney (b) and Perth (c) wave scenarios. First buoy is placed (300,300) and is fixed, but the second buoy is turned around the first one by the 360◦ and a distance between 50(m) and 300(m). The powerful configurations are characterized by the colors.

4 Meta-Heuristic Search Techniques

All of the heuristic methods that are compared in this paper are listed in Table 2. All proposed approaches are run with the same parallel computational resources according to the descriptions in the previous section. The type of parallelism (per-individual and per-frequency (PF)) is shown in the second column of Table 2. We can categorize the listed methods in two distinct groups: population-based and single-solution optimizers. In the first group, we assess the performance of Differential Evolution [22] (DE) and Covariance-Matrix Adaptation Evolutionary Strategies [10] (CMA-ES), as very well-established paradigms of EAs; in addition, PE [15] is a partial-evaluation search technique that tries to optimize the layouts based on partial information provided by sampling uniform random subsets of the frequencies. As the probability crossover rate (P_{cr}) of DE play an important role, we test three different values. We evaluate CMA-ES using both parallelism techniques (per frequency and per-individual).

It was observed in [15] that population-based methods tended to perform poorly for the 16 buoy layouts due to the low number of full evaluations possible within the time budget. In contrast, methods that built or refined a single layout performed better. These include variations on 1+1EA's including those that adjusted the mutation step size (fixed, linear, dynamic (Rechenberg's $1/5^{th}$ Success Rule [23]) and fuzzy adaptive). Even more successful were new methods that incrementally built a single layout one buoy at a time. These methods had the advantage of reducing the average number of buoy interactions in early evaluations, thus allowing a greater number of function evaluations within the time budget. Some of these methodologies, including LS_1-NM_{2D} and LS-NM$_{\text{allDims}}$ used the Nelder-Mead simplex search to refine initial placements. However, the most effective methods, which include, smart local search, (SLS) and variants of improved smart local search (ISLS), are newly described in this paper and use randomized local sampling.

These are the search methods listed in the last nine rows of this table, The algorithms that perform better for larger farm layouts ($N = 16$) are described next.

4.1 Smart Local Search (SLS)

It has been demonstrated in [15] that the performance of the iterative Local Search (LS-NM) algorithm for placing buoys one-at-a-time is more efficient than a range of methods for optimizing buoy placements all-at-once. It was observed in this previous work that a good candidate position for the next buoy is in the neighborhood of the previous buoy. The SLS improves upon these earlier searches by placing the next buoy in a relative position informed by peaks in the power landscape built from sampling positions in a two-buoy model under local wave conditions. Examples of such landscapes are given in Figure 3 which shows a 3D power landscape of the simplified irregular, Sydney, and Perth wave models. It can be seen from these landscapes that, even for two buoys, there is variation in the shape of the landscape and the positions of the point at which there are constructive interactions. Note that, for a given wave regime, is it not practical to infer the shape of this power landscape by means other than sampling it. Additionally, the inter-relationship among the absorbed power, angle and distance between two-buoy layout for different wave scenarios

Algorithm 1 *SmartLocalSearch*

procedure SMART LOCAL SEARCH
Initialization
Generate surrogate 2-buoy power model
$size = \Omega$ ▷ Farm size
$pos = [(x_1, y_1), \ldots, (x_N, y_N)] = \perp$ ▷ positions
$pos(1) = (size/2, 0)$
Search
for i in $[1, .., N]$ **do**
update search sectors S
$bestEnergy = 0$
$bestPosition = (0, 0)$
for j in $[1, ..15]$ **do** ▷ 15 random samples
$(x_s, y_s) = U(S)$ ▷ sample sectors
$pos(i) = (x_s, y_s)$
$energy = Eval(\mathbf{pos})$
if $energy > bestEnergy$ **then**
$bestEnergy = energy$
$bestPosition = (x_s, y_s)$
end if
end for
$pos(i) = bestPosition$
end for
return pos ▷ Final Layout
end procedure

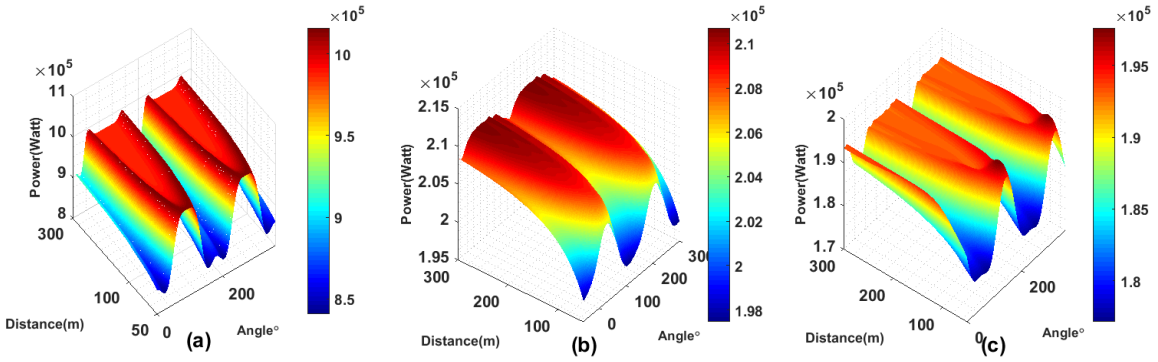

Figure 4: A 3D power landscape, for relative angle and distance between two buoys based on the simplified irregular wave model (a) and two real wave scenarios: Sydney (b) and Perth (c). Note that there are ridges in the power landscape corresponding to areas of constructive interference. The Improved Smart Local Search algorithm variants, described in this paper, exploit this local landscape when placing buoys.

Table 2: Summary of the search methods used in this paper. All methods are given the same computational budget. Parallelism can be expressed as per-individual or per-frequency depending on the number of individuals in the population from section.4.

Abbreviation	Parallelism	Description
R-S	per-frequency	Random Search
$\text{PE}_{50\,\mu}$	per-individual	Partial Evaluation[24], all frequencies (PE-FULL), population $\mu \in \{10, 50, 100\}$
$\text{PE}_{f\,\mu}$	per-individual	Partial Evaluation [24], partial frequencies, $f \in \{1, 4, 16\}$, $\mu \in \{10, 50, 100\}$
TDA	per-individual	Algorithm for optimizing wind turbine placement from [25]
CMA-ES	per-individual	CMA-ES[10] all dimensions, $\mu =' 4+int(3*log(D))$ndim , $\sigma = 0.17*size$
CMA-ES_{PF}	per-frequency	All settings are like CMA-ES
CMA-ES (2+2)	per-individual	Setup for CMA-ES from [12], $\sigma = 20m$
CMA-ES_{PF} (2+2)	per-frequency	All settings are based on [12]
$\text{DE}_{P_{cr}}$	per-individual	Differential evolution [22], $\mu = 50$, $F = 0.5$, $P_{cr} \in \{0.3, 0.5, 0.7, 0.9\}$
1+1EA_{σ}	per-frequency	1+1EA(all dimensions), mutation step size with $\sigma \in 3, 10, 30$(m)
1+1EA_{s}	per-frequency	1+1EA (all dimensions) with uniform mutation in range $[0, s]$ with $s = 30m$ from [12]
$\text{1+1EA}_{\text{Linear}}$	per-frequency	1+1EA (all dimensions) with linearly decaying mutation step size [15]
$\text{1+1EA}_{1/5}$	per-frequency	1+1EA (all dimensions) with adaptive step size [26]
Fuzzy-1+1EA	per-frequency	1+1EA (all dimensions) with fuzzy adaptive mutation step size
Iterative-1+1EA	per-frequency	Iterative local search - buoys are placed in sequence using best of local neighborhood search [15]
$\text{LS-NM}_{\text{allDims}}$	per-frequency	Local search + Nelder-Mead search in all Dimensions [15]
NM_Norm_{2D}	per-frequency	Buoys placed in sequence using Nelder-Mead search, Initial placement normally distributed from last buoy position [15]
NM_Unif_{2D}	per-frequency	Buoys placed randomly and then refined using Nelder-Mead Initial placement uniformly distributed from last buoy position [15]
LS_1-NM_{2D}	per-frequency	Local Sampling + Nelder Mead search. Buoys placed at random offset from previous buoy and placement refined by Nelder-Mead search. [15]
LS_3-NM_{2D}	per-frequency	Iterative local search + Nelder-Mead search. Placements sampled at 3 random offsets from previous location, best placement used as starting point for Nelder-Mead search. [15]
SLS	per-frequency	Providing the two-buoy power landscape+ Extracting a proper domain of the distances and the angles +Iterative local search +Smart Mutation;Uniform distribution, 15 samples, step= $rand(R'$, Buo$y_{Distance} + \kappa_2(20m))$. 4.5 folds faster than the best method of the prior study [15] for 16-buoy layout.
SLS-NM	per-frequency	Smart Local Search with three samples of the mutation+ Nelder-Mead search
ISLS	per-frequency	Improved Smart Local Search : Creating a more accurate knowledge-based surrogate power model, placing a new buoy: the initial sequential N_{sb}-buoy number $\sigma = R'$ and for next buoys $\sigma = 2 \times R'$: Mutating:10 samples for initial sequential N_{sb}-buoy number, and for next buoys 20 samples, $step = rand(R'$,Buo$y_{Distance}$+10m). 60% faster than LS_3-NM_{2D}in [15] for 16-buoy layout.
ISLS-NM	per-frequency	Improved Smart Local Search (10 samples) for the initial sequential N_{sb}-buoy number and for last buoys 3 samples + Nelder-Mead search,
ISL$S_{(II)}$-F	per-frequency	Improved Smart Local Search (for initial sequential N_{sb}-buoy number) (3 samples)+ Applying SQP (for finding the furthest point of the area based on the layout position). 20 times faster than the best method of the prior work [15] for 16-buoy layout.
ISL$S_{(II)}$-NM	per-frequency	Improved Smart Local Search(II) (for initial sequential N_{sb}-buoy number) 3 samples + Nelder-Mead Search.
ISL$S_{(II)}$-SQP	per-frequency	Improved Smart Local Search(II) (for initial sequential N_{sb}-buoy number) 3 samples + Sequential Quadratic Programming Search.
ISL$S_{(II)}$-AS	per-frequency	Improved Smart Local Search(II) (for initial sequential N_{sb}-buoy number) 3 samples + Active-Set Search.
ISL$S_{(II)}$-IP	per-frequency	Improved Smart Local Search(II) (for initial sequential N_{sb}-buoy number) 3 samples + Interior-Point Search.

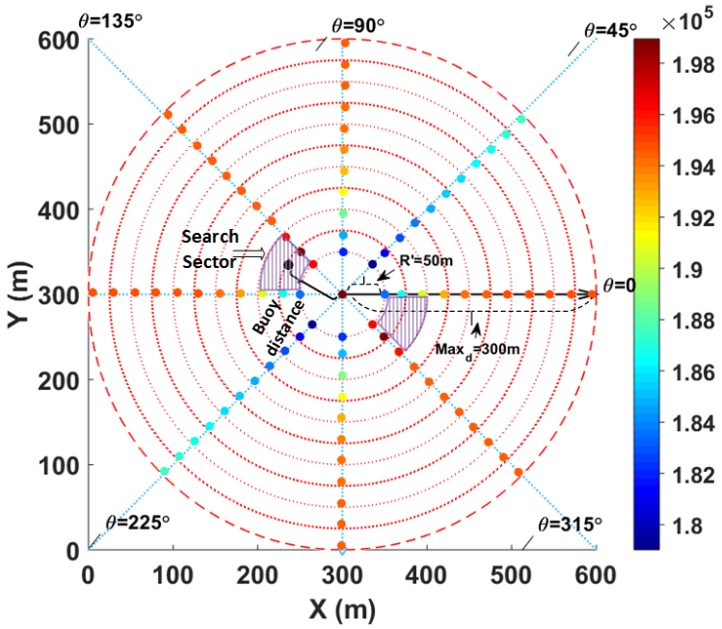

Figure 5: The 2D power landscape of two-buoy array based on the Adelaide wave scenario. The power configurations are characterized by the colors.

can be seen in Figure 4. In the SLS method, this two-buoy power landscape was sampled. The pattern of sampling into this landscape is shown in Figure 5. This sampling landscape has an angular resolution of 45 degrees intervals and a distance resolution of 5m intervals. This sampled landscape is computationally cheap to build because it models interactions between only two buoys. Moreover, this sampling exercise only has to be run once for each wave scenario at the beginning of the search process. These samples are then used to define the most promising sectors, called the *search-sectors*, in the search landscape for the placement of the next buoy. These sectors, marked in Figure 5 with a dotted line, lie between the best and second-best points in the search landscape on either side of the current buoy.

For the placement of each buoy, a local search makes 15 samples, uniformly distributed in the search sectors (subject to boundary constraints). These samples are assessed with the full model, which calculates *all* buoy interactions in the current array. From these 15 samples, the best buoy location is selected. Careful analysis of our experiments has shown that 15 samples have been sufficient to improve upon the initial placement with a probability of 99% with an expected improvement of power production almost identical to that of a much larger number of samples. The detailed of the buoy placement and sampling can be seen in the Algorithm 1.

4.2 Smart Local Search + Nelder-Mead (SLS-NM)

The Smart Local Search + Nelder-Mead (SLS-NM) explores the same search sectors as the SLS algorithm defined above. The SLS-NM algorithm differs in that it takes only three random samples from the search sectors and uses the best of these as the start point for a Nelder-Mead (NM) simplex search process. This search process can robustly move to a local optimum from its starting point. In order to fit within the computational budget, the number of steps (evaluations) in the NM search is limited to 20. To verify that this number of steps is adequate we ran a longer experiment with 120 evaluations for each NM search (Figure 6) and we found that, in most cases, the improvement from the extra evaluations was less than 2% of the power output for that buoy. Moreover, where there was a significant improvement it happened only after a prohibitively large number of evaluations.

4.3 Improved Smart Local Search (ISLS)

From the careful analysis of experimental runs using the SLS methods, we made three observations.

1. The search sector containing the best-sampled positions was always in the direction of the opposite side of the farm.

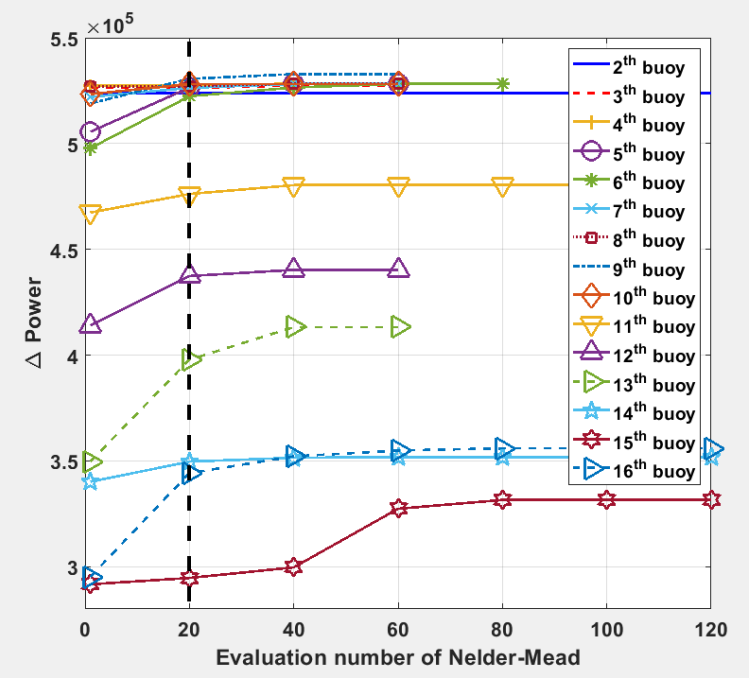

Figure 6: The impact of Nelder-Mean evaluation number on the SLS performance (16-buoy) for the Perth wave model.

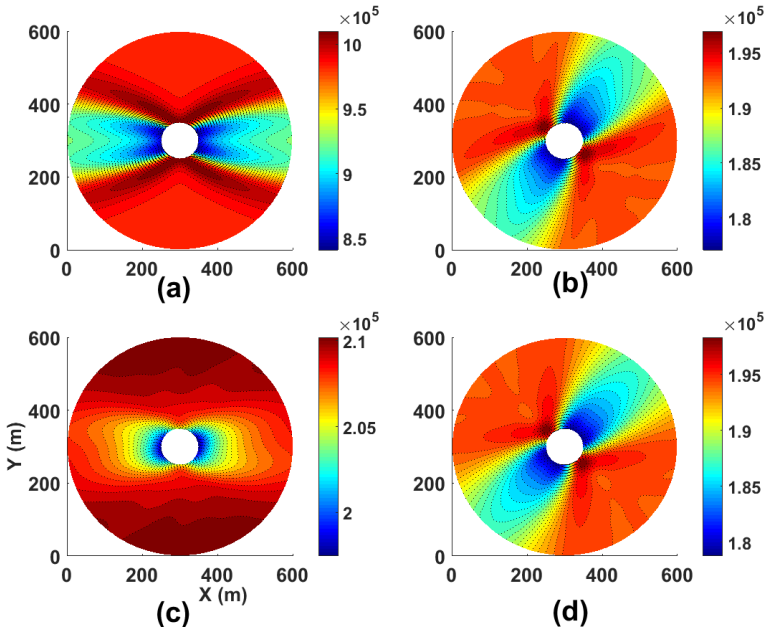

Figure 7: The 2-buoy power landscape of four different wave scenarios including simplified irregular (a), Perth (b), Sydney (c) and Adelaide (d). The landscapes are characterized by colors.

2. The best samples from the SLS-NM method came from a sector which was narrower in angular extent but longer in radial extent (this can be observed in the detailed landscapes in Figure 7).

3. The search space for placing the next buoy becomes much harder after hitting the top boundary of the farm. This is due to occlusion from the front row of buoys.

4. The placement of the first buoy in the center of the bottom boundary of the farm can be sub-optimal if the best angle for the alignment of buoys in the surrogate power landscape causes some buoys to encounter the left or right boundary of the farm.

In response to these observations, we designed a refined search method called Improved Smart Local Search (ISLS). This search method addresses the first observation above by only sampling the search sector in the direction of the current opposite boundary of the farm (upwards in our implementation). This improves search efficiency. ISLS addresses the second observation above by restricting the angular extent of the search sector to 22.5 degrees in the direction of the second-best sample and doubling the radial extent of the search sector. The third observation above is addressed by reducing the number of samples used when placing buoys on the first sweep to the opposite farm boundary (phase 1) and deploying the time-budget thus saved to running more samples to place subsequent buoys (phase 2). Lastly, the fourth observation is addressed by placing the first buoy in the left corner of the landscape if the best angle is between zero and 90 degrees and in the right corner otherwise.

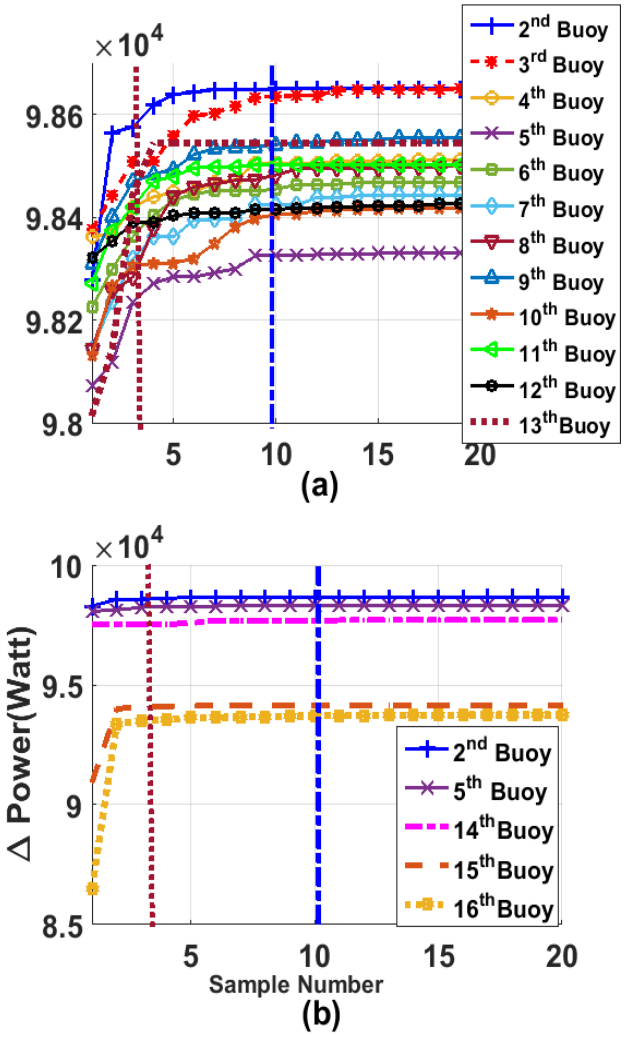

Figure 8: The impact of sample number on the ISLS performance (16-buoy) for the Perth wave model. The red vertical line shows 3-sample.

The decision on the number of samples to use in the first sweep of buoy placement (phase 1) and then for the placement of subsequent buoys (phase 2) is based on empirical studies on the impact of different numbers of samples in the different wave scenarios. To illustrate the findings of this process, Figure 8(a) shows the average power gain from sampling for the first 12 buoys for ten runs in the Perth wave scenario. The red and blue vertical lines, respectively, indicate the average power gained after three and ten samples. For the experiments generating the figure, the buoys

were placed according to the best result obtained after 20 samples. The figure indicates that for the placement of the first 12 buoys (phase 1) the curves flatten after ten samples, with buoy three showing the largest gain, after 10 samples, of 0.018%. This indicates that there is not much to be gained from sampling the real power landscape beyond this point. Thus for phase 1, 10 samples were allocated for each buoy placement. For the placement of the last four buoys (phase 2), as illustrated in 8(b) the gain from sampling is steeper and, for buoy 16, the improvement between 10 and 20 samples is 0.032%.

A second notable feature of Figure 8(a) is that the power curves for some buoys are vertically displaced relative to others. This indicates that for some buoy placements the power landscape is more challenging. In general, we have observed that the displacement of these sampling curves for later buoys is dependent on the placement of previous buoys. In some experiments we have observed that this dependence on placement history can even lead to some minor anomalies in search behavior where sampling *less* for earlier buoy placements appears to make the search landscape slightly easier for subsequent buoy placements. However, we have observed for all wave regimes that the best *median* performance for wave farms is obtained by employing as many samples as the time budget allows in both phases of the search process.

4.4 Improved Smart Local Search Nelder-Mead (ISLS-NM)

As previously noted, due to occlusion by other buoys, the power landscape for phase 2 of the search is different to that encountered for phase 1. This means that, for phase 2 buoy placements, the search sector from the surrogate power landscape might not contain the best location for the placement of the next buoy. In order to allow a broader search of the power landscape a variant of ISLS, called ISLS-Nelder-Mead (ISLS-NM) was created. This variant has an identical phase 1 search to ISLS but in phase 2 it performs a local search with three samples followed by 20 samples of Nelder-Mead search starting at the best of these three sampled locations. In almost all experimental runs these 20 samples were enough to converge to a point where the step size is less than 1% of the total power output for that buoy.

4.5 Improved Smart Local Search-II (ISLS-II)

For both SLS and ISLS the placement of the first buoy starts in the center of the bottom boundary of the farm area. This starting position was intended to give a degree of flexibility in the layout of buoys in the farm, thus allowing some freedom for subsequent buoys to be placed to the left or right of this starting position so as to extract maximum energy. However, for ISLS the search sector in phase 1 of placements is always in a consistent direction (left-or-right) from the starting point. This means that, to maximize the number of placements possible in a rectangular area of a farm it makes sense to place the first buoy in the bottom corner of the farm where the choice of the corner is in the opposite direction to the search sector. That is, if the search sector is to the upper right of the current buoy then the first buoy should be placed in the bottom left of the farm. Likewise, if the search sector is to the upper left then the first buoy should be placed in the bottom right of the farm. This informed choice of placement is the basis of the final variants of placement algorithms described here. These algorithms are called Improved Smart Local Search-II (ISLS$_{II}$).

Indeed, in SLS and ISLS, after creating the surrogate power model, the search-sector boundaries should be determined which are including the proper angles based on the distance resolution. This process is involved in observing the surrogate power model, extracting the knowledge of best angles per distances, transforming this knowledge into some rules for sampling part that are manually done by a user. For dealing with the drawback, a simple automated reasoning technique is recommended for generalizing the proposed method. This simple algorithm, by comparing all angles for each distance of the power model based on the absorbed powers of the layout, produces a rules table. Each row of the table represents the distances range and the suitable range of angles are shown in the columns which configurations are able to produce more power. This table is employed for optimizing larger arrays.

Once the search sector is determined, each of these variants has an identical first phase to ISLS using the ten-sample randomized local search within the search sector that is defined by a surrogate landscape.

The only difference in this phase was the placement of the first buoy in the corners of the bottom of the farm rather than the center. In the second phase of the search, a number of search variants were used for the placement of final buoys. Each of these variants, in their second phase, still begin by identifying the best of three random sample positions in the search sector relative to the previously placed buoy. The variants differ in the type of search that proceeds from this sample point. These variants are shown in the final five rows of Table 2. We describe these variants next.

ISLS-II + Active Set (ISLS$_{II}$-AS) Refines the placement of each buoy with 20 evaluations of the Active-Set [27] search method. This method identifies the set of boundary constraints that are relevant to the current state of search and concentrates search close to these. This method is able to take large steps through the search space, thus allowing for quick coverage of the search area (Algorithm 2).

ISLS-II + Sequential Quadratic Programming(ISLS$_{II}$-SQP) Refines the placement of each buoy by performing Sequential Quadratic Programming (SQP) [28]. This search method deploys Newton's method when the search is away from boundary constraints and reverts to constrained search when boundaries are encountered.

Algorithm 2 $ISLS(II) - AS$

procedure IMPROVED SMART LOCAL SEARCH(II) + ACTIVE-SET
Initialization
  Generate surrogate 2-buoy power model
  $size = \Omega$ ▷ Farm size
  $pos = [(x_1, y_1), \ldots, (x_N, y_N)] = \perp$ ▷ positions
  if $0° < bestLocalAngle < 90°$ **then**
    $pos(1) = (0, 0)$
  else
    $pos(1) = (size, 0)$
  end if
  $buoyNum = 2$
Search
  update search sector S
  while $bottomYBoundary(S) < size$ **do** ▷ phase 1
    $bestEnergy = 0$
    $bestPosition = (0, 0)$
    for j in $[1, .., 10]$ **do** ▷ 10 random samples
      $(x_s, y_s) = U(S)$ ▷ sample sector
      $pos(i) = (x_s, y_s)$
      $energy = Eval(\mathbf{pos})$
      if $energy > bestEnergy$ **then**
        $bestEnergy = energy$
        $bestPosition = (x_s, y_s)$
      end if
    end for
    $pos(i) = bestPosition$
    $buoyNum = BouyNum + 1$
    update search sector S
  end while
  for i in $[buoyNum, .., N]$ **do** ▷ phase 2
    $bestEnergy = 0$
    $bestPosition = (0, 0)$
    for j in $[1, ..3]$ **do** ▷ 3 random samples
      $(x_s, y_s) = U(S)$ ▷ sample sector
      $pos(i) = (x_s, y_s)$
      $energy = Eval(\mathbf{pos})$
      if $energy > bestEnergy$ **then**
        $bestEnergy = energy$
        $bestPosition = (x_s, y_s)$
      end if
    end for
    $bestPosition = ActiveSearch(bestPosition, 20)$
    $pos(i) = bestPosition$
    update search sector S
  end for
  return pos ▷ Final Layout
end procedure

ISLS-II + Fast placement (ISLS$_{II}$-F) We observed in the earlier ISLS-NM that the phase 2 buoy placements tended to reside on the lee-side behind the front row of buoys, with these buoys finishing far from each other. Informed by this observation the ISLS$_{II}$-F algorithm uses 20 iterations of SQP search to place each buoy, one at a time,

Table 3: Summary of the best achieved 4-buoy layout per experiment (Power (Watt)) for the real wave scenarios .

Sydney wave model				
Methods	**DE**	**CMA-ES**	**LS_3-NM_{2D}**	**ISL$S_{(II)}$-AS**
Max	412667	**412705**	412294	409350
Median	412557	412488	411069	409281
Mean	412580	412477	410839	409246
Std	63	140	1184	110
Perth wave model				
Max	398844	**399607**	396759	395525
Median	395898	399607	392753	391517
Mean	396615	399117	391361	391898
Std	1415	1033	5543	1275
Adelaide wave model				
Max	399431	**402278**	401858	398032
Median	397176	402278	398352	394131
Mean	395620	402073	396106	394604
Std	4271	709	6685	1523
Tasmania wave model				
Max	1093468	**1094611**	1094524	1079485
Median	1090833	1094611	1079619	1072041
Mean	1090734	1094611	1079429	1071853
Std	1985	0.0072	10432	3135

at a position that is the maximum Euclidean distance from the previously placed buoys. Note that by using Euclidean distance rather than an energy model makes evaluating buoy positions particularly fast compared to other variants.

ISLS-II + Nelder-Mead (ISLS$_{II}$-NM) Similar to the earlier ISLS-NM this algorithm applies 20 iterations of the Nelder-Mead algorithm to the placement of each buoy.

ISLS-II + Interior point algorithm (ISLS$_{II}$-IP) This algorithm refines each buoy position using the interior point (IP) algorithm [29] for constrained search. This method is similar to other active-set methods above except that boundaries are approximated using barrier functions which allow search near constraint boundaries rather than on constraint boundaries.

This concludes our description of the different buoy placement algorithms explored in this paper. The next session presents detailed results comparing the performance of these algorithms.

5 Experimental Results

This section presents the results of the experiments comparing the performance of the algorithms described above on the placement of buoys under the different wave scenarios. In this section, we present a quick summary of the results for 4-buoy layouts before progressing to the much more challenging 16-buoy layouts. As mentioned previously for the 16 buoy-layout problems the full computational budget of 3 days on 12 CPU cores was used wherever possible. In order to make a fair comparison, an equivalent number of evaluations was used for the 4-buoy layout problem.

5.1 4-buoy layout results

Table 3 summarises the results of the four best-performing search methods on the 4-buoy layout problem in the four real wave scenarios. The output for the search method with the best maximum performance in each wave scenario is highlighted in bold. It can be seen from this table that the best results for each of the four methods shown are within 2% of each other in terms of raw performance. All methodologies are able to produce layouts with a q-factor close to one. However, it is also clear from these results that the global CMA-ES method consistently has the best performance across all wave scenarios and the variation in this performance is quite narrow.

The 4-buoy layouts produced by these methods for the four real wave scenarios is shown in Figure 9. The buoys are colored based on their individual output. From these layouts, we can observe that, except for the Sydney wave scenario, all buoys form a row with the spacing and orientation varying with the wave environment. The orientation of this row (in the Perth, Adelaide and Tasmania scenarios) is approximately aligned to the norm of the predominant wave direction

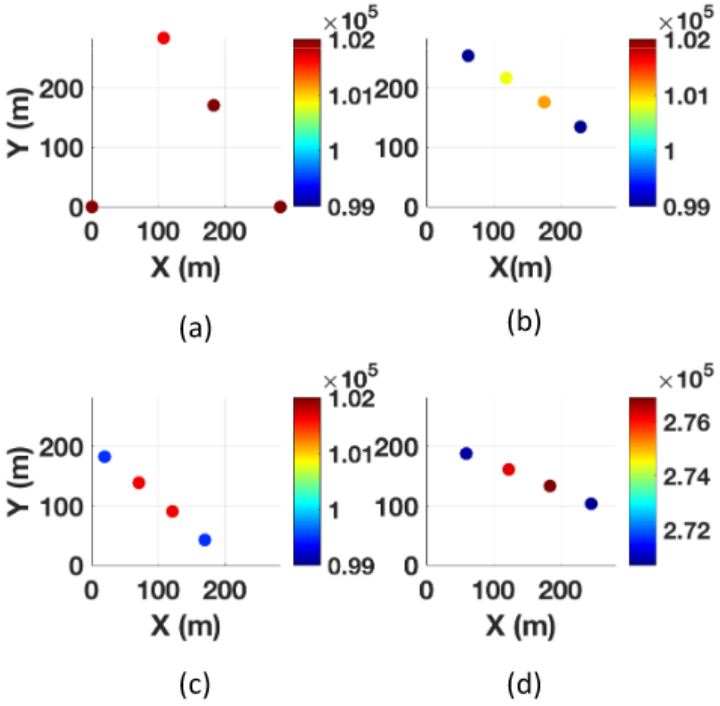

Figure 9: The best 4-buoy layouts of the real wave scenario by CMA-ES (a) (Sydney: Power=412705 (Watt), q-factor=0.975), (b) (Perth: Power=399607, q-factor=1.0366), (c) (Adelaide: Power=402278, q-factor=1.036) and (d) (Tasmania: Power=1094611, q-factor=1.0334).

for each scenario. It can also be seen that the middle two buoys in these three layouts also produce slightly more energy than the outer buoys. This is due to constructive interactions between buoys. The layout for the Sydney wave scenario differs markedly in its spacing and orientation. The Sydney wave environment is more varied in terms of wave direction and, thus, opportunities to exploit constructive interactions through a static layout are much reduced. As a result, our optimization runs produced layouts where the buoys are well-spaced, which minimizes destructive interactions.

5.2 16-buoy layouts

Compared to the 4-buoy layout problem, the 16-buoy layout problem is challenging in terms of both problem constraints and computational budget. The farm area for the 16-buoy layout is larger than that for the 4-buoy layout, but not so large as to allow all 16 buoys to be placed in a single line in any wave scenario. Moreover, the cost of the evaluative model scales quadratically with the number of buoys. This means the number of full evaluations of a 16-buoy layout within the 3-day time budget is limited to approximately 300.

This additional problem complexity, coupled with limited computational budget heavily favors search algorithms tailored to the details of this problem domain. This is illustrated, for the simplified irregular wave scenario in Figure 10. This box-and-whiskers plot demonstrates the best-achieved power for a 16-buoy layout of each search framework. The new methods described in this paper are given in the last nine columns of the chart. The improved performance of these new search methods is quantified in Table 4. From these results it can be seen that the most reliably performing placement algorithms are among variants of ISLS$_{(II)}$ with a run of ISLS$_{(II)}$-AS producing the best maximum performance with a layout power of 7878917 Watts (marked in bold). In terms of statistical significance, the Active-Set, Nelder-Mead, and Fast-Search variants of ISLS$_{(II)}$ perform significantly better than the non ISLS$_{(II)}$ search methods with $p < 0.025$ over the 10 trial runs using a one-tailed Wilcoxon ranked-sum test. Moreover the other ISLS$_{(II)}$ variants: SQP and Interior-Point perform better than all but the ISLS-NM search method.

In contrast with the 4-buoy problem, the methods which place buoys one at time dominate over global search methods in terms of achieving the best performance within the given computational budget. Figure 11 shows how the convergence of the new algorithms presented in this paper compares with the best search algorithms from [15], which was based on the $1 + 1$EA.

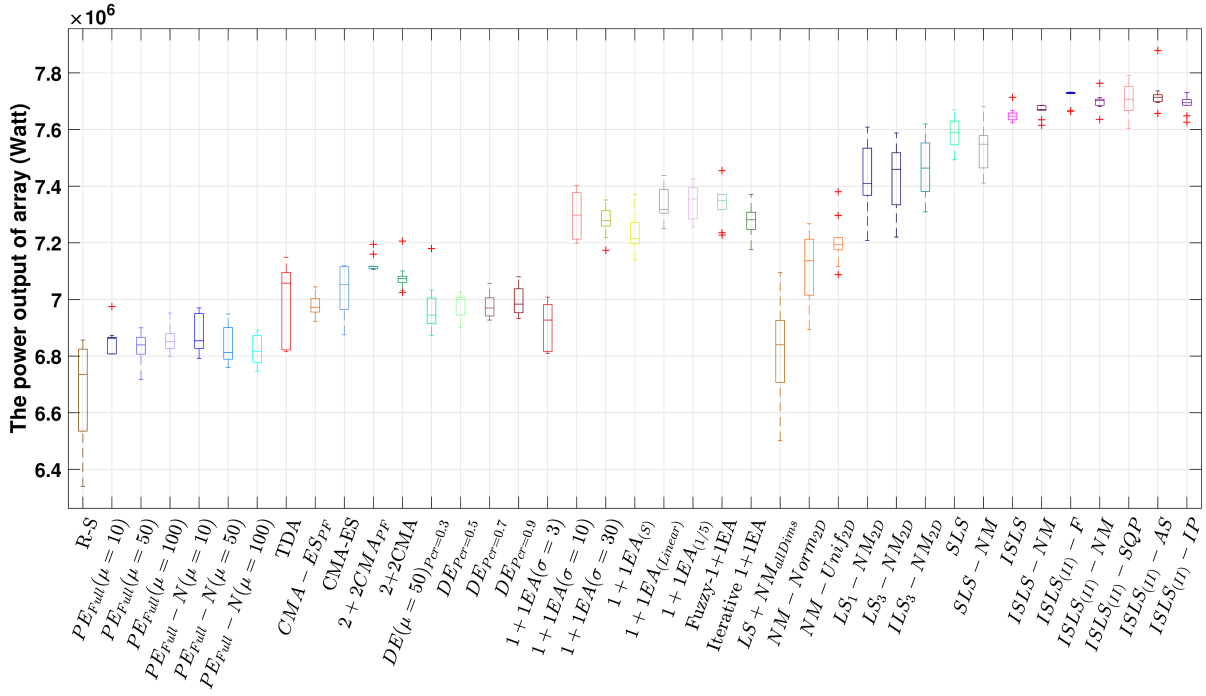

Figure 10: The comparison of proposed heuristic approaches for optimizing the position of WECs. (ISLS$_{(II)}$-AS) method can enhance the 16-buoy layout power on average at **4%** compared with the best result of LS-NM [15] for the simplified wave scenario.(best layout per run)

Table 4: The performance comparison of various heuristics for the 16-buoy case(best solution per run) (Std = standard deviation) with the simplified irregular wave model.

Methods	**PE-Full (Uniform)**			**PE-Full(Normal)**			**DE**		
	$\mu = 10$	$\mu = 50$	$\mu = 100$	$\mu = 10$	$\mu = 50$	$\mu = 100$	$P_{cr} = 0.3$	$P_{cr} = 0.5$	$Pcr = 0.9$
Max	6974948	6900024	6952017	6957388	6948746	6892210	7179681	7025873	7079962
Median	6859475	6839557	6851342	6853987	6812866	6816282	6944795	6999356	6983523
Mean	6856337	6821864	6860037	6869586	6837972	6822553	6971231	6981195	6994172
Std	48701	61880	50377	61153	70048	52911	89244	41931	48943
Methods	**1+1EA**						NM_{2D}		**Iter-(1+1)EA**
	Mu-s=3	Mu-s=10	Mu-s=30	Linear	1/5 rule	Fuzzy	Uniform	Normal	
Max	7008380	7402584	7351112	7437481	7425665	7454922	7380318	7267242	7370972
Median	6927230	7297465	7278120	7317408	7354589	7348676	7193110	7136712	7354589
Mean	6908203	7292035	7275118	7330286	7343858	7335624	7205098	7108693	7274989
Std	83157	77794	51745	60803	59690	67061	83944	116380	54380
Methods	**LS$_1$-NM$_{2D}$**	**TDA**	**CMA-ES**	**R-S**	**1+1EA$_S$**	**(2+2)CMA-ES**	**LS$_3$-NM$_{2D}$**	**LS$_1$-NM$_{allDims}$**	**SLS**
Max	7608600	7148655	7118996	6825723	7370389	7205956	7587758	7094642	7669439
Median	7409029	7057564	7053351	6658523	7214263	7073295	7459614	6839911	7590039
Mean	7427027	7005873	7038352	6676831	7236977	7080011	7426742	6823836	7587410
Std	129780	133977	84859	63883	67406	49771	123603	198512	52538
Methods	**SLS+NM**	**ISLS**	**ISLS-NM**	**ISLS$_{II}$-F**	**ISLS$_{II}$-NM**	**ISLS$_{II}$-SQP**	**ISLS$_{II}$-AS**	**ILS$_3$-NM$_{2D}$**	**ISLS$_{II}$-IP**
Max	7680161	7713744	7685633	7730799	7763249	7790679	**7878917**	7619404	7730844
Median	7548235	7647335	7670401	7723825	7702161	7706788	7714011	7463928	7694381
Mean	7537582	7651360	7666201	7721954	7698639	7701115	**7724370**	7469493	7688422
Std	81727	25635	23437	9773	31790	60012	58341	102760	30453

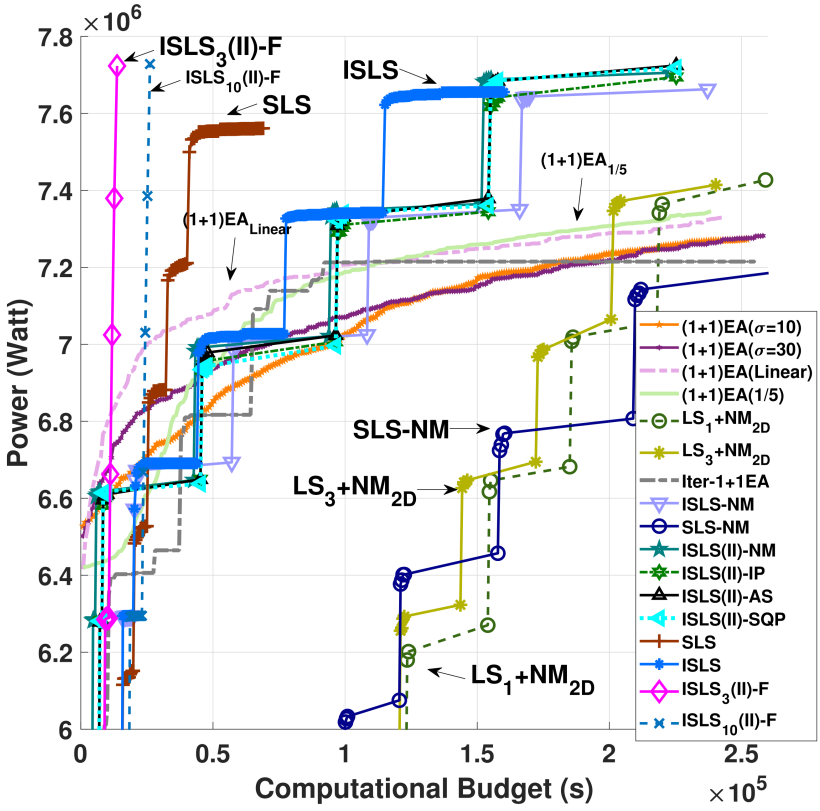

Figure 11: A comparison of the average convergence rate of the proposed methods with the work [15] for 16-buoy layout over 72 hours (simplified irregular wave model). The average fitness value of the best individuals in each population were recorded for each method.

Table 5: The performance comparison of the new search ideas with LS_1-NM_{2D} [15] for 16-buoy arrays and simplified irregular wave scenario. All methods are given the same computational budget, 3 days, 12 processors. Parallelism can be expressed as per-frequency.

Proposed Methods	**Best layout** (%)	**Mean performance** (%)
SLS	0.8%	2.16%
SLS-NM	0.94%	1.49%
ISLS	1.38%	3.02%
ISLS-NM	1.01%	3.22%
ISL$S_{(II)}$-F	1.62%	3.91%
ISL$S_{(II)}$-NM	2.03%	3.66%
ISL$S_{(II)}$-SQP	2.39%	3.69%
ISL$S_{(II)}$-AS	**3.55**%	**4**%
ISL$S_{(II)}$-IP	1.6%	3.52%

Table 6: Summary of the best achieved power per experiment (Watt) for real wave scenarios (16-buoy layout)

Sydney wave model					
Methods	**DE**	**CMA-ES**	**LS_3-NM_{2D}**	**ISL$S_{(II)}$-F**	**ISL$S_{(II)}$-AS**
Max	1507235	1512337	1524915	1509037	**1534883**
Median	1499663	1505254	1512190	1498963	1531785
Mean	1499901	1505705	1511814	1499663	1531491
Std	3207	2770	6421	3440	2339
Perth wave model					
Max	1440344	1443893	1516098	1537788	**1565836**
Median	1436441	1433949	1472851	1529076	1550877
Mean	1435539	1434333	1470658	1528225	1549409
Std	4171	4626	26990	9016	16920
Adelaide wave model					
Max	1449967	1461741	1525144	1551102	**1583052**
Median	1444455	1445241	1497211	1547351	1578797
Mean	1443442	1446621	1477342	1548027	1573476
Std	3757	5879	57675	1796	11694
Tasmania wave model					
Max	3901664	3916983	4090733	4180781	**4241838**
Median	3868558	3886093	4005319	4105700	4218894
Mean	3867923	3882930	3999507	4115758	4213652
Std	22588	19705	69758	26696	21775

Each curve plots the evolution of the average of the best individual over the three days of computational budget. The search parameters used by most algorithms are tuned to take advantage of most of the search budget. The exceptions to this are the plain SLS and ISLS algorithms where the local sampling converges early and the 3-sample and 10 sample versions of ISLS$_{(II)}$-F which place the last buoys very quickly with a fast distance-based proxy function. From the plots, it can be seen that all the other variants of ISLS$_{(II)}$ converge to a very similar level of performance in a very similar time to each other. The average performance of all of ISLS$_{(II)}$ variants is above all others. Overall, the best performing variant: ISLS$_{(II)}$-AS extracts 4% more power than the previous best published algorithm: LS$_1$+NM$_{2D}$ (Table 5). This small difference in performance equates to approximately $175,000 US dollars in extra annual avenue for the wave farm. [1]

5.2.1 Real Wave Scenarios

To see how algorithm performance translates to real wave scenarios we ran 10 trials each for five selected search methods (DE, CMA-ES, LS$_3$NM$_{2D}$, ISLS$_{(II)}$-F, ISLS$_{(II)}$-AS) for 16-buoy layouts on the Sydney, Perth, Adelaide and Tasmania wave scenarios. Table 6 outlines the results of these runs. The ISLS$_{(II)}$-AS performed significantly better than the other four methods with $p < 0.025$ over the 10 trial runs using a one-tailed Wilcoxon ranked-sum test.

These results are reflected in the box-and-whiskers charts for each of the methods for the different wave scenarios shown in Figure 12. This figure shows a clear margin between the performance of ISLS$_{(II)}$-AS and the other methods. It can be seen that ISLS$_{(II)}$-F varies greatly in its performance between scenarios with a much poorer performance for Sydney. This perhaps reflects on diminished usefulness for the distance-based proxy function in this complex wave environment. To sum up, in all cases, ISL$S_{(II)}$-AS provides the best mean and maximal power output among the five compared algorithms statistically. As an example, ISL$S_{(II)}$-AS is able to overcome DE, CMA-ES, LS_3-NM_{2D}, and ISL$S_{(II)}$-F for 16-buoy farm at 9.00%, 7.00%, 6.51%, and 1.64% respectively where the Adelaide wave scenario is applied. A comparison of the ISLS$_{(II)}$-AS convergence rate with four other methods for Perth wave model can be seen in Figure 13. The figure illustrates that ISLS$_{(II)}$-F has the highest convergence speed; however, the average quality of proposed 16-buoy layouts of ISLS$_{(II)}$-AS can be considerably better.

The best 16-buoy layouts produced by ISLS$_{(II)}$-AS in each of the four-wave scenarios are shown in Figure 14. For Perth, Adelaide and Tasmania the layouts are similar with the buoys being oriented in a line roughly normal to the prevailing wave direction with buoys placed in phase 1 (lower numbers) forming a bottom row and the buoys placed in phase 2 (higher numbers) behind these. It can be seen that fewer buoys are placed in phase 1 for Tasmania than for

[1] Based on an annualized average wholesale price of US $65 per MWh average for the Australian market in 2017/18.

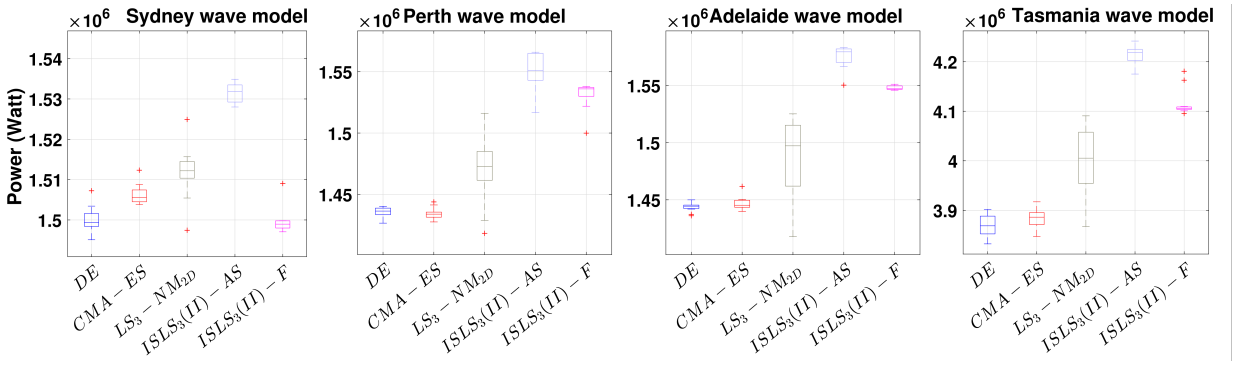

Figure 12: The optimization results of the proposed algorithms based on the best layout per run for 16-buoy and four real wave scenarios. ISL$S_{(II)}$-AS is able to overcome other well-known methods.

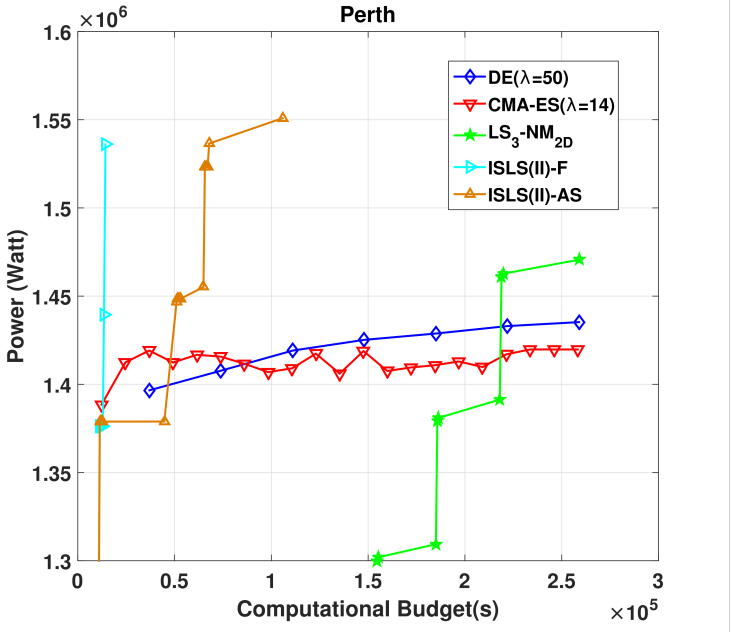

Figure 13: The average convergence rate comparison of the proposed methods for N=16 in Perth wave model.

Adelaide. This appears to be due to an interaction between the wave orientation and the shape of the farm – with the Adelaide layout better aligned to the diagonal of the farm area. The layout produced for the Sydney wave scenario is very different from the with a row for phase 1 oriented to the east and the other buoys being placed at large distances from the others. This pattern was observed for a number of Sydney runs where the best layouts tended to contain widely dispersed buoys to minimize destructive interference.

The impact for constructive and destructive interference in each environment can be visualized in the trajectory of average q-factor as ISLS$_{(II)}$-AS places buoys in each of the wave scenarios. Figure 15 shows this trajectory for the four wave scenarios and, as a reference to the simplified irregular wave scenario. It can be seen that Adelaide, Perth, and Tasmania are characterized by constructive interference in phase 1 and both Adelaide and Perth still have a q-factor greater than one even after phase 2. In contrast, the Sydney wave scenario is characterized by destructive interference throughout the search – though still producing net gains in power output for each buoy placed.

One interesting observation from the layouts in Figure 9 is that there are buoys on the end of the front row for both Adelaide and Tasmania which produce less energy than the buoys closer to shore. This, slightly counter-intuitive, the result is due to complex interactions between the front row of buoys and ocean waves. Figure 16 demonstrates the nature of these interactions by showing the power landscape for the Perth wave scenario for four different layouts. In all

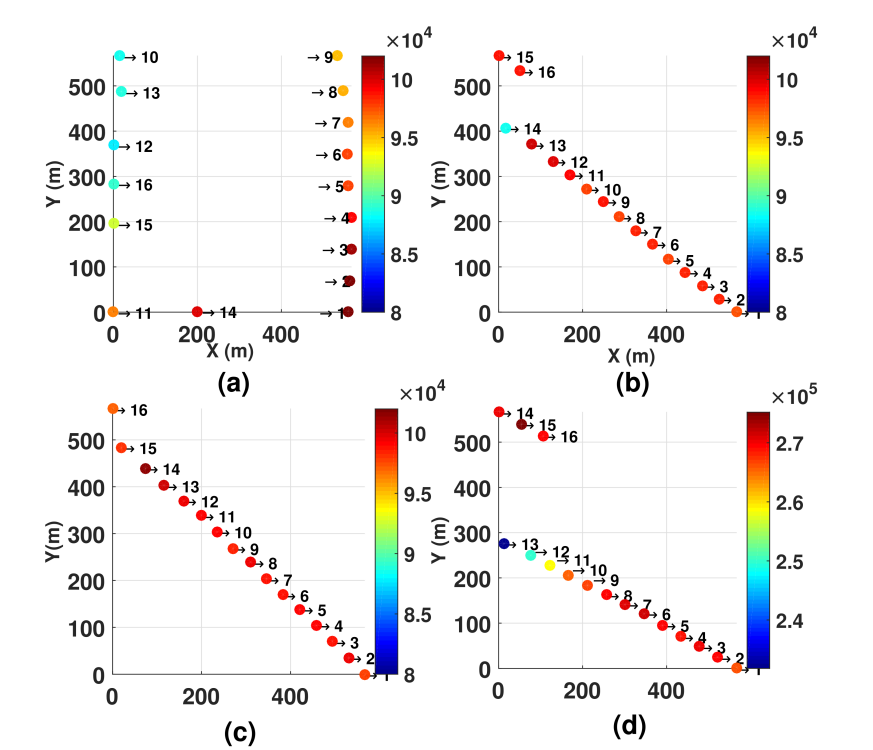

Figure 14: The best-founded 16-buoy layouts of the real wave scenarios by ISL$S_{(II)}$-AS (a) (Sydney: Power=1534883 (Watt), q-factor=0.9068), (b) (Perth: Power=1565657, q-factor=1.015), (c) (Adelaide: Power=1583052, q-factor=1.019) and (d) (Tasmania: Power=4241838, q-factor=1.0012).

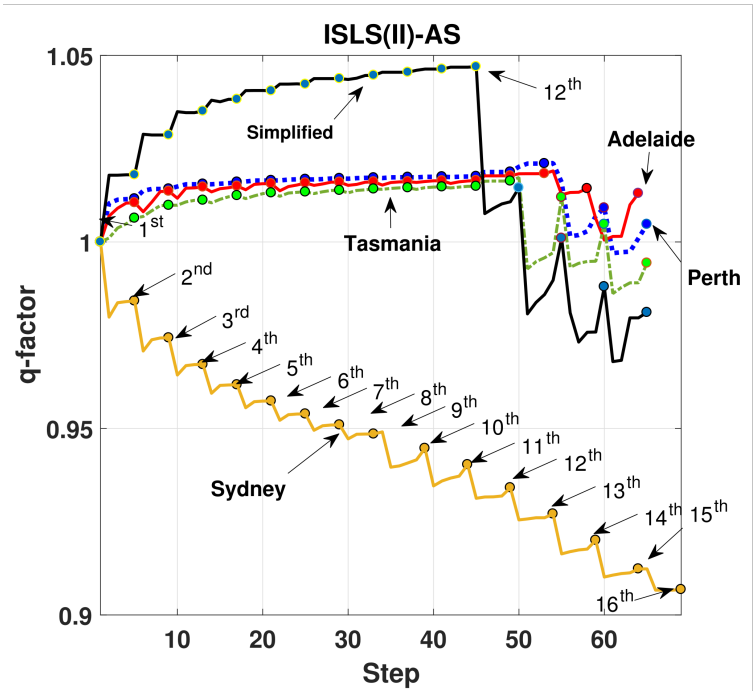

Figure 15: The average of ISLS(II)-AS q-factor performance (16-buoy) for real wave models and the simplified.

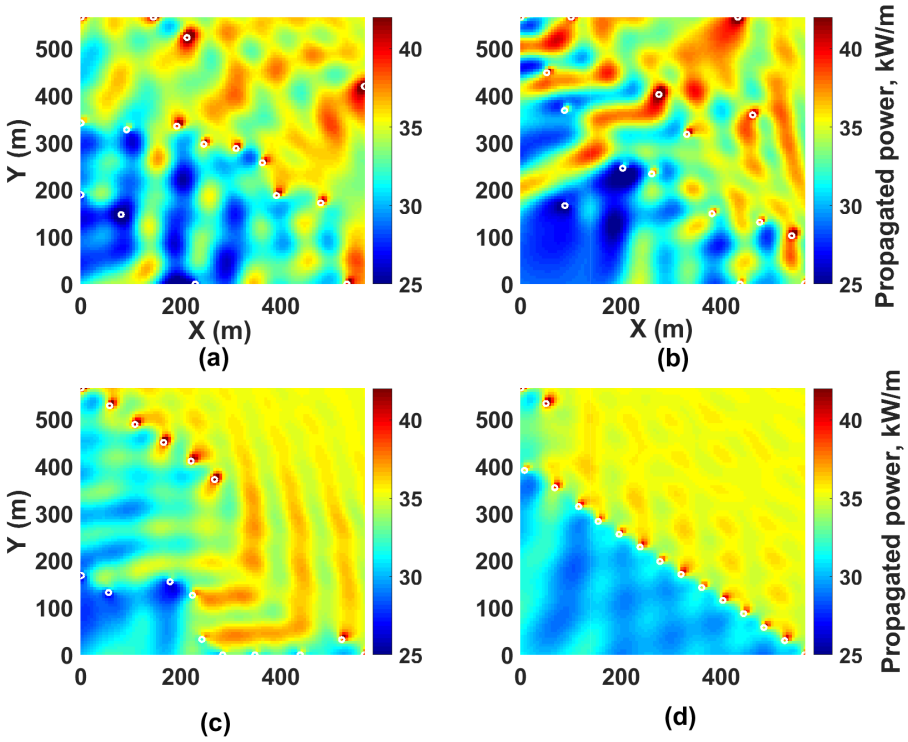

Figure 16: The wave interpolation of the best 16-buoy layouts for Perth wave scenario, a) CMA-ES, b) DE, c) LS-NM and d) ISLS(II)-AS. White circles represent the buoys placement.(the wave angle propagates at 232.5 degrees).

cases, the wave energy in the area in the lee of the front row of the buoys (top right) is greater than the area immediately in front. This phenomenon is due to the fact that buoys interact strongly with the surrounding environment on all sides. In fact, modeling over an extended area shows that the damping influence of these layouts stretches more than 500 meters further out to see than the buoy array. This extended impact helps illustrate the potential for even relatively small buoy arrays to extract energy from a relatively large area of ocean. Consequently, It is clear to see except ISLS$_{(II)}$-AS, other methods can not place all buoys correctly in the right placements (some buoys are located in the dark blue area).

6 Conclusion

This work has explored algorithmic solutions to the problem of placing wave-energy converter buoys in arrays in order to maximize energy output. We have developed, evaluated, and systematically compared nine new search heuristics to a range of existing standard and domain-specific search techniques.

The algorithms were benchmarked on the problems of producing in 4 and 16-buoy layouts in both artificial and real wave scenarios.

Producing effective layouts presented interesting challenges in terms of the high cost of full function evaluations (approx 700 seconds for 16 buoys) but also complex problem dynamics including multi-modal constructive and destructive interference between buoys and highly varied power landscapes for buoy placement.

In this work, the algorithms that performed best in experiments were hybrid search heuristics that used local search informed by inexpensive proxy models that were customized for local conditions. These methods further optimized the cost of function evaluations by placing one buoy at a time – thus minimizing the number of modeled interactions. The most effective search techniques of all used the proxy model to inform the placement of the first buoy and switched to a combination of local search and gradient search techniques once the farm boundary was reached.

One possible limitation of the best approaches described here is that they allow no backtracking to further optimize buoy positions once they have been placed. Preliminary experiments with further global optimization of four buoy layouts have shown some small potential gains from further global optimization, though at much much greater (87-

Table 7: The comparison of 4-buoy layouts achieved by a larger search-sector and different sample numbers (Power (Watt)) for the Perth wave scenario.

Perth wave model						
Methods	**DE**	**CMA-ES**	**L**S_3**-N**M_{2D}	**ISL**$S_{(II)_3}$**-AS**	**ISL**$S_{(II)_{10}}$**-AS**	**ISL**$S_{(II)_{20}}$**-AS**
Max	398844	**399606**	395525	398690	399253	399304
Median	397895	**399606**	391517	397223	398620	399215
Mean	397158	398657	391898	397127	398666	**399152**
Std	1359	1229	1275	1259	386	154

fold) computational cost and a slightly greater farm extent. The optimization results of this investigation (a larger search-sector) for Perth wave scenario can be seen in Table 7.

This work can be extended in a number of ways. First, while the hydrodynamic models employed here are state-of-the-art in terms of fidelity, the wave farm environments are still simplified in terms of farm geometry (assumed to be square) and seafloor topography (assumed to be uniform depth). In the future, both of these assumptions can be relaxed with farm geometry allowed to vary to match realistic lease-boundaries and the hydrodynamic model updated to allow varied seafloor depth. It is also possible to increase the complexity of the model for each buoy in terms of size, depth, and tether parameters. Some of these parameters impact on cost and, thus, produce scope for multi-objective optimization. Finally, there is scope to learn a robust and accurate proxy function for evaluating energy outputs. Such an approach might use machine learning techniques such as Deep Neural Network to act as a partial or complete estimator function for the output of a given layout. Such an estimator has the potential to greatly increase the speed of search and open the way for further improvements in search heuristics.

Acknowledgements

Our work was supported by the Australian Research Council project DE160100850 and the supercomputing resources provided by the Phoenix HPC service at the University of Adelaide..

References

[1] B Drew, A R Plummer, and M N Sahinkaya. A review of wave energy converter technology. *Proceedings of the Institution of Mechanical Engineers, Part A: Journal of Power and Energy*, 223(8):887–902, 2009.

[2] Tom W Thorpe et al. *A brief review of wave energy*. Harwell Laboratory, Energy Technology Support Unit, 1999.

[3] A. D. De Andrés, R. Guanche, L. Meneses, C. Vidal, and I. J. Losada. Factors that influence array layout on wave energy farms. *Ocean Engineering*, 82:32–41, 2014.

[4] L. D. Mann, A. R. Burns, , and M. E. Ottaviano. Ceto, a carbon free wave power energy provider of the future. In *the 7th European Wave and Tidal Energy Conference (EWTEC)*, 2007.

[5] N. Y. Sergiienko, B. S. Cazzolato, B. Ding, and M. Arjomandi. Three-tether axisymmetric wave energy converter: estimation of energy delivery. In *Proceedings of the 3rd Asian Wave and Tidal Energy Conference*, 2016.

[6] B. F. M. Child and Vengatesan Venugopal. Optimal configurations of wave energy device arrays. *Ocean Engineering*, 37(16):1402–1417, 2010.

[7] C. Sharp and B. DuPont. Wave energy converter array optimization: A review of current work and preliminary results of a genetic algorithm approach introducing cost factors. In *ASME 2015 International Design Engineering Technical Conferences and Computers and Information in Engineering Conference*, pages V02AT03A025–V02AT03A025. American Society of Mechanical Engineers, 2015.

[8] C. Sharp and B. DuPont. Wave energy converter array optimization: A genetic algorithm approach and minimum separation distance study. *Ocean Engineering*, 163:148–156, 2018.

[9] P. Ruiz, V. Nava, M. B. R. Topper, P. R. Minguela, F. Ferri, and J. P. Kofoed. Layout optimisation of wave energy converter arrays. *Energies*, 10(9):1262, 2017.

[10] N. Hansen. The cma evolution strategy: a comparing review. *Towards a new evolutionary computation*, pages 75–102, 2006.

[11] K. N. Krishnanand and D. Ghose. Glowworm swarm optimization for simultaneous capture of multiple local optima of multimodal functions. *Swarm Intelligence*, 3(2):87–124, 2009.

[12] J. Wu, S. Shekh, N. Y. Sergiienko, B. S. Cazzolato, B. Ding, F. Neumann, and M. Wagner. Fast and effective optimisation of arrays of submerged wave energy converters. In *Genetic and Evolutionary Computation Conference (GECCO)*, pages 1045–1052. ACM, 2016.

[13] Dídac Rodríguez Arbonès, Boyin Ding, Nataliia Y Sergiienko, and Markus Wagner. Fast and effective multi-objective optimisation of submerged wave energy converters. In *International Conference on Parallel Problem Solving from Nature*, pages 675–685. Springer, 2016.

[14] Dídac Rodríguez Arbonès, Nataliia Y. Sergiienko, Boyin Ding, Oswin Krause, Christian Igel, and Markus Wagner. Sparse incomplete lu-decomposition for wave farm designs under realistic conditions. In *Parallel Problem Solving from Nature – PPSN XV*, pages 512–524, Cham, 2018. Springer.

[15] M. Neshat, B. Alexander, M. Wagner, and Y. Xia. A detailed comparison of meta-heuristic methods for optimising wave energy converter placements. In *Genetic and Evolutionary Computation Conference (GECCO)*, pages 1318–1325. ACM, 2018.

[16] Marcos Blanco, Marcos Lafoz, Dionisio Ramirez, Gustavo Navarro, Jorge Torres, and Luis Garcia-Tabares. Dimensioning of point absorbers for wave energy conversion by means of differential evolutionary algorithms. *IEEE Transactions on Sustainable Energy*, 2018.

[17] Australian wave energy atlas @ONLINE, June 2016.

[18] Carnegie Clean Energy. Ceto 6 design update @ONLINE, November 2017.

[19] G. Wu. Radiation and diffraction by a submerged sphere advancing in water waves of finite depth. In *Proc. of the Royal Society of London A: Mathematical, Physical and Engineering Sciences*, volume 448, pages 29–54. The Royal Society, 1995.

[20] F. F. Flavià, A. Babarit, and A. H. Clément. On the numerical modeling and optimization of a bottom-referenced heave-buoy array of wave energy converters. *International Journal of Marine Energy*, 19:1–15, 2017.

[21] N Yu Sergiienko. Frequency domain model of the three-tether wecs array, 2016.

[22] R. Storn and K. Price. Differential evolution–a simple and efficient heuristic for global optimization over continuous spaces. *Journal of global optimization*, 11(4):341–359, 1997.

[23] A. Auger. Benchmarking the (1+1) evolution strategy with one-fifth success rule on the bbob-2009 function testbed. In *Proceedings of the 11th Annual Conference Companion on Genetic and Evolutionary Computation Conference: Late Breaking Papers*, pages 2447–2452. ACM, 2009.

[24] Duc-Cuong Dang and Per Kristian Lehre. Runtime analysis of non-elitist populations: From classical optimisation to partial information. *Algorithmica*, 75(3):428–461, 2016.

[25] Markus Wagner, Jareth Day, and Frank Neumann. A fast and effective local search algorithm for optimizing the placement of wind turbines. *Renewable Energy*, 51:64–70, 2013.

[26] Á. E. Eiben, R. Hinterding, and Z. Michalewicz. Parameter control in evolutionary algorithms. *IEEE Transactions on evolutionary computation*, 3(2):124–141, 1999.

[27] J. Nocedal and S. J. Wright. *Nonlinear Equations*. Springer, 2006.

[28] C. L. Xiao and H. X. Huang. Optimal design of heating system for rapid thermal cycling mold using particle swarm optimization and finite element method. *Applied Thermal Engineering*, 64(1-2):462–470, 2014.

[29] M. Glavic and L. Wehenkel. Interior point methods: A survey, short survey of applications to power systems, and research opportunities. *University of Liège, Belgium*, 2004.